Numerical Modeling of Micromixing Performance of Five Generic Microchannel Reactors using Villermaux/Dushman Competing Test Reaction

Peyvand Valeh-e-Sheyda * ⓘ**, Majid Yarmohammad** ⓘ

1. Department of Chemical Engineering, Kermanshah University of Technology, Kermanshah, Iran. E-mail: p.valeh-sheyda@kut.ac.ir
2. Department of Chemical Engineering, Kermanshah University of Technology, Kermanshah, Iran. E-mail: e.majidyarmohammadi2014@gmail.com

ARTICLE INFO	ABSTRACT
	Microchannel reactors, known as high-process intensification reactors, are utilized in various fields due to their intensive micromixing performance, which is crucial for fast chemical reactions. The work presented here depicts the Computational Fluid Dynamics (CFD) modeling of five generic microchannel reactors (MCRs), namely T-square, T-trapezoidal, Y-rectangular, concentric, and caterpillar designs based on the experimental published data of the parallel competing Villermaux-Dushman reaction. The main objective of this study is to numerically quantify the effects of the total liquid flow rate (1-18 mL/min), micromixer dimension (150-1600 µm), and configuration on the values of the pressure drop, energy dissipation, mixing time, and segregation index (XS). The CFD results revealed that under constant concentrations of the reactants ($C_{H_2BO_3^-,0}$, $C_{H^+,0}$, $C_{I^-,0}$, $C_{IO_3^-,0}$ = 0.091, 0.0224, 0.016, 0.0033 M), the dissipation rate intensified with increasing the total flow rate but weakened with the change in symmetry and the channel diameter. Further, the estimated values of the segregation index illustrated that the caterpillar design could bring about a reasonable enhancement in micromixing performance with energy dissipation (ε) and segregation index of 1335700 W/kg and 0.0024, followed by T-square and Y-rectangular with Xs~ 0.0061 and 0.0161, respectively. The low values of mixing time for caterpillar MCR were found in the range of 0.01-0.1 s for liquid flow rates of 1-18 mL/min.

Introduction

Over the past decades, microfluidics at the molecular scale have played a significant role in many chemical reactions in continuous flow mode. The technique is considered to be a safe and friendly environment as compared to the bench-top processes. Regarding the significance of effective mixing, the researchers have paid much attention to develop guidelines for characterizing the flow and mixing performances at the molecular scales in microfluidics. The Villermaux/Dushman reaction system, the most frequently employed experimental scheme in parallel instantaneous reactions, scales the mixing rate at the molecular level [1]. The

---

* Corresponding Author: P. Valeh-e-Sheyda (E-mail address: p.valeh-sheyda@kut.ac.ir)

micromixing at the molecular scale directly affects the chemical reaction and the yields of desired products [2]. Furthermore, accurate information on the flow pattern and concentrations of reaction species, as well as the characterizing processes for flow parameters, can be rarely attained via empirical procedures in the existing microscopic-size of microfluidics.

Table 1. The main simulation examples in the MCRs utilizing Villermaux/Dushman parallel competitive reaction

Micromixers' type & scale	Resulting Information	Ref
An asymmetrical T-shaped micromixer	(1) One-dimension scale-up in the horizontal direction can benefit from less deterioration to micromixing performance. (2) The Re No. can be used as a fundamental criterion to adjust the width of the mixing channel according to the operational capacity.	[11]
Hartridge-Roughton T-shaped tube Y-shaped tube 1mm×2 mm	(1) Hartridge-Roughton mixing device is the most efficient. (2) The Y-shaped tube is characterized by a poor micromixing intensity	[12]
Tube in tube MCR with a pore size of 20 µm	(1) X_S decreased with rising Re No. and declining the flow ratio. (2) The optimal values of porous diameter and width of the annular channel were found to be 20 µm and 250 µm to enhance the micromixing efficiency.	[13]
Pore-array intensified coaxial double-tube MCR, 0.3-0.4 mm,	The optimal micromixing time in the micromixing reactor could reach 0.06 ms.	[14]
A 3D serpentine microchannel 23 mm×200, 300, and 400 µm ×125 µm	A stronger inertia force could lead to a more robust transversal flow and higher mixing efficiency.	[3]
A 3D serpentine microchannel with a periodic vortex-inducing structure, 50 µm	The maximum vortex intensity reached 1563 s^{-1}, as Re increased to 102.	[15]
T-type with ultrasound wave, 900 µm ×950 µm	The segregation index improved up to 10-20% by the piezoelectric transducer.	[16]
countercurrent-flow microchannel reactor, 1 mm	The micromixing time was estimated as 0.0002~0.0018 s within the *Re* range of 200~1400, which is much quicker than most conventional mixing devices.	[4]

In recent years, Computational Fluid Dynamics (CFD) models with acceptable precision have been demanded for numerical simulation of the reactive flow and local micromixing processes [3]. So far, many studies have developed CFD models to explain the observed mixing

characterization and investigate the mass transfer efficiency and mixing phenomena in microchannels, including asymmetrical T-type and Y-type microchannels based on the iodide-iodate reaction system [4, 5]. To overcome the constraints on the microchannel length, various numerical studies on micromixing performance were performed in more complex MCRs, including the curved, T-mixer with square bends, split-and-recombine, 3D-shape, and serpentine MCRs [6-10] utilizing Villermaux/Dushman parallel competitive reaction. Table 1 summarizes the numerical simulation examples of micromixing in MCRs, and the resulting information on the current competing parallel reactions for characterizing micromixing in different microfluidics structures.

The micromixing performance of the competitive-parallel Villermaux/Dushman reactions was also developed in the laminar regime for Reynolds numbers in the range 60-300, utilizing both a conventional CFD approach and a novel lamellae-based model [17]. The result indicated that the promising lamellar solution requires extremely fine computational grids to resolve sharp concentration gradients. The CFD simulations based on the iodide-iodate test reaction in a single countercurrent-flow microchannel reactor illustrated that under various operating conditions, an optimal outlet length results in a balance between micromixing efficiency and energy saving [4].

Recently, the homogeneous mixing, as well as the energy consumption, were experimentally investigated for distinct sorts of microchannels with different geometrical structures applying the Villermaux/Dushman parallel-competitive method [18]. However, the detailed numerical evaluations on the effect of the configuration of microfluidics on the mass transfer and flow characteristics received far less attention. Under this motivation, in the present study, a CFD model was established as support for previous experimental observations to characterize and verify the micromixing quality in five microfluidics with various geometries. To better understand the mixing quality and the place of the contact point inside the MCRs, the values of computational pressure, energy dissipation, micromixing time, segregation index, as well as the mass fraction of the by-products were examined at different ranges of total liquid flow rate for the five configurations of micromixers. The achieved results bring a guide for the design and optimization of the operating conditions to satisfy the mixing demands of particular chemical processes.

Methods for Micromixing Investigation

Villermaux/Dushman Reaction System

The competitive parallel Villermaux/Dushman system mainly comprises three reactions: (1) typical parallel competitive reactions of the quasi-instantaneous neutralization reaction, (2) the fast redox reaction, and (3) quasi-instantaneous equilibrium [19].

$$H_2BO_3^- + H^+ \rightarrow H_3BO_3 \qquad \text{(quasi-instantaneous)} \qquad (1)$$
$$5\,I^- + IO_3^- + 6H^+ \rightarrow 3I_2 + 3H_2O \qquad \text{(very fast)} \qquad (2)$$
$$I_2 + I^- \leftrightarrow I_3^- \qquad \text{(quasi-instantaneous equilibrium)} \qquad (3)$$
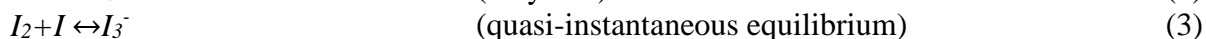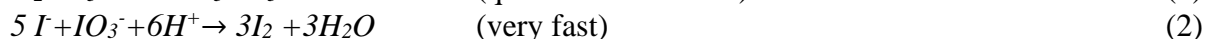
Assuming perfect micromixing conditions, the acid is homogeneously dispersed and instantaneously consumed by the borate ions, H_2BO_3, to form boric acid, H_3BO_3, so the reaction (2) does not occur. Ultimately, the iodine ions, I_3^-, are produced in the reaction between iodine (I_2) and iodide ions (I^-), as indicated by Eq. 3. The reaction rates are presented as follows:

$$r_1 = k_1[H^+][H_2BO_3^-] \qquad k_1 = 1 \times 10^{11} \qquad \text{(L.mol}^{-1}.\text{s}^{-1}\text{)} \qquad (4)$$
$$r_2 = k_2[H^+]^2[I^-]^2[IO_3^-] \qquad \text{Log}\,k_2 = 9.28105 - 3.664\sqrt{I} \qquad \text{(for } I \leq 0.166 \text{ M)} \qquad (5)$$
$$\text{Log}\,k_2 = 8.383 - 1.5112\sqrt{I} + 0.237\,I \qquad \text{(for } I \geq 0.166 \text{ M)} \qquad (6)$$

$$I = 1/2 \sum_{i=1}^{n} c_i Z_i^2 \tag{7}$$

where k_2 is measured relative to the ionic power (I) of the solution, and I is a function of ion concentration in the solution (c) and their amount of charge, z.

$$r_3 = r_3^+ - r_3^- = k_3^+ \, [I^-][I_2] - k_3^- [I_3^-] \qquad k_3^+ = 5.9 \times 10^{\,9} \text{ L.mol}^{-1}.\text{s}^{-1} \tag{8}$$

$$k_3^- = 7.5 \times 10^6 \text{ s}^{-1} \tag{9}$$

The calculated value of I is assumed to be 1.01393, based on the laboratory work of Azimi et al. [20]. The segregation index, X_s, employed to identify the efficiency of micromixing, takes a value between zero for an ideal mixed system and one for a fully-segregated system. It is described by the following expression:

$$X_S = \frac{Y}{Y_{ST}} \tag{10}$$

$$Y = \frac{4(C_{I_2} + C_{I_3^-})}{C_{H,0^+}} \tag{11}$$

$$Y_{ST} = \frac{6C_{IO_{3,0}^-}}{6C_{IO_{3,0}^-} + C_{H_2BO_{3,0}^-}} \tag{12}$$

where Y represents the ratio of moles consumed by Reactions 2 and 3 to the total acid moles in the feed, and Y_{ST} is the value of Y in the case of complete separation. Besides, the zero subscripts in the above two relations (Eqs. 11 and 12) indicate the initial concentration of each component before introducing the mixing region.

Microchannel geometry

Fig. 1 displays the five configurations of the microfluidics used for numerical simulations, corresponding to the microfluidic devices designed in the previous laboratory study [18]. According to the figure, the microchannel reactors have square, trapezoidal, rectangular, and circular cross-section areas with internal diameters varying from 150-1600 µm.

(a)

(b)

(c)

(d)

(e)
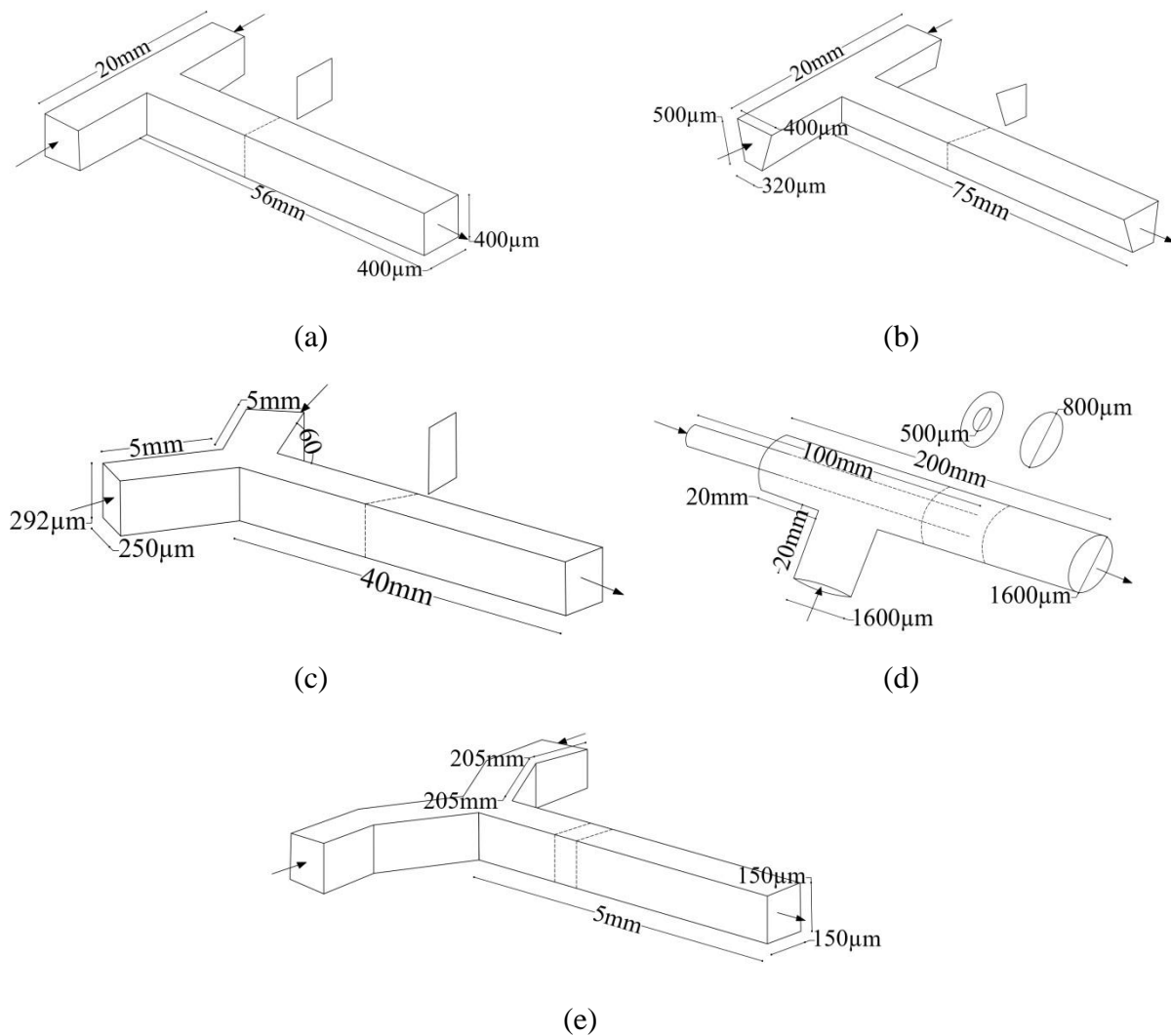
Fig. 1. Geometric dimension for the studied MCRs: (a) T-square (b) T-trapezoidal (c) Y-rectangular (d) Concentric (e) Caterpillar [18]

CFD Modeling Features

Geometry and Grid Generation

The geometries are discretized with a high-quality grid system according to the three-dimensional mesh. As a result of the presence of numerical diffusion, a preliminary test of grid dependency was accomplished for four particular grid numbers varying from 1.6×10^3 to 1.8×10^5. The final values of the segregation index were computed at the exit of the MCR for every grid system. The predicted results using different grids showed that the mixing index varied significantly with the change in grid numbers. Finally, it is found that a further increase of nodes in the range from 1.0×10^4 to 1.6×10^5 produces a negligible difference in the value of the defined variable. As such, for all the configurations studied, the geometries of the entire MCRs were descritisized based on the tetrahedral and triangular mesh with no less than ~10,000 elements. The mesh characteristics, as well as the optimum grid numbers, are presented in Table 2.

Table 2. Grid characteristics for the five devices

Microchannel Configuration	Optimum Grid Numbers	Mesh Type
T-square	10866	Tetrahedral
T-trapezoidal	31348	Tetrahedral
Y-rectangular	20089	Triangular/ Tetrahedral
Concentric	169133	Triangular/Tetrahedral
Caterpillar	35883	Tetrahedral

Mathematical Model

The incompressible model includes numerical solutions of steady Navier-Stokes conservation equations for continuity, momentum, and species. Due to the small dimensions, the fluid flow is dominated by laminar flow patterns, and the gravity effect is considered insignificant in all numerical methods. The model used examines the mixing of the buffer solution of $H_2BO_3^-$, I^-, and IO_3^- at one inlet with diluted sulfuric acid at the other. The following equations depict the changes in momentum, mass, and concentrations of each species:

Continuity equation:

$$\Delta.\mathbf{u} = 0 \tag{13}$$

Momentum equation:

$$\rho\left[\frac{\partial\mathbf{u}}{\partial t} + (\mathbf{u}.\nabla)\mathbf{u} = -\nabla p + \mu\nabla^2\mathbf{u}\right] \tag{14}$$

Species equation:

$$\frac{\partial(\rho_i)}{\partial t} + \nabla.(\rho_i\mathbf{u}) = \nabla.(D_i\nabla\rho_i) + r_i \qquad i= H^+, H_2BO_3^-, I^-, IO_3^-, I_2, I_3^- \tag{15}$$

where u(m/s) represents the velocity vector, p (Pa) denotes the pressure, μ (kg/m.s) is the fluid viscosity, ρ (kg/m^3) displays the fluid density, t (s) is the time, ρ_i, and D_i are the mass concentration and diffusion coefficient of species i, and r_i is the formation rate of species i, that is produced by the chemical reaction.

Initial and Boundary Conditions

The initial gauge pressure and temperature set to 0 Pa and 300 K, respectively. The velocity-inlet and the pressure outlet were assigned as the boundary conditions at the microchannel inlet and outlet, respectively. Besides, no-slip boundary conditions were set for the solid walls. To investigate the mixing performance numerically, the concentrations of the two currents, including a buffer solution of $H_2BO_3^-$, I^-, and IO_3^- and diluted sulfuric acid, were considered with constant volume intensity at the two ends of the microchannel inlet. The initial concentrations for the two inlets were assigned based on the concentrations presented in Table 3.

Table 3. Concentrations of the reactants used for numerical simulations of the Villermaux-Dushman test reaction in MCRs

Inlet	$C_{H_2BO_3^-,0}$ [M]	$C_{H^+,0}$ [M]	$C_{I^-,0}$ [M]	$C_{IO_3^-,0}$ [M]
1	0.091	0	0.016	0.0033
2	0	0.0224	0	0

CFD Modeling Strategy

For all the physical models presented in this simulation, the computational package COMSOL Multiphysics 5.1 (COMSOL Inc., Stockholm, Sweden) was applied to solve the differential equations of momentum and mass transport by the finite element method. The values of density, ρ, and viscosity, μ, of the fluids were determined at the temperature and pressure corresponding to water in the software. Initial relative pressure and temperature were applied at 0 Pa and 300 K, respectively. The flow rate of 10 mL/h was considered constant for the acid solution, while it was varied in the range of 1 to 18 mL/h for the other reactants in the micromixer inlet. Computing the Reynolds number of various total flow rates, the flow regime was considered an incompressible laminar flow inside the MCRs. To define the reaction kinetics, the reaction equations were defined separately using the Transport of concentrated species model. Incompressible Navier-Stokes equations for momentum and fluid mass transfer and reaction in steady state were solved numerically, simultaneously. The solution was considered to have achieved convergence when the residuals of all equations were less than 10^{-4}.

Results and Discussion

Pressure Drop

To validate the numerical methodology utilized for characterizing micromixing, the present values of computational average pressure drops were calculated and compared with the published quantitative experimental data (Fig. 2) [18]. As reported in the literature, the changing dependence in the pressure drop along the axial direction of the MCR determines the mixing region [21]. In addition, a high-pressure loss is usually connected with high-quality micromixing [20].
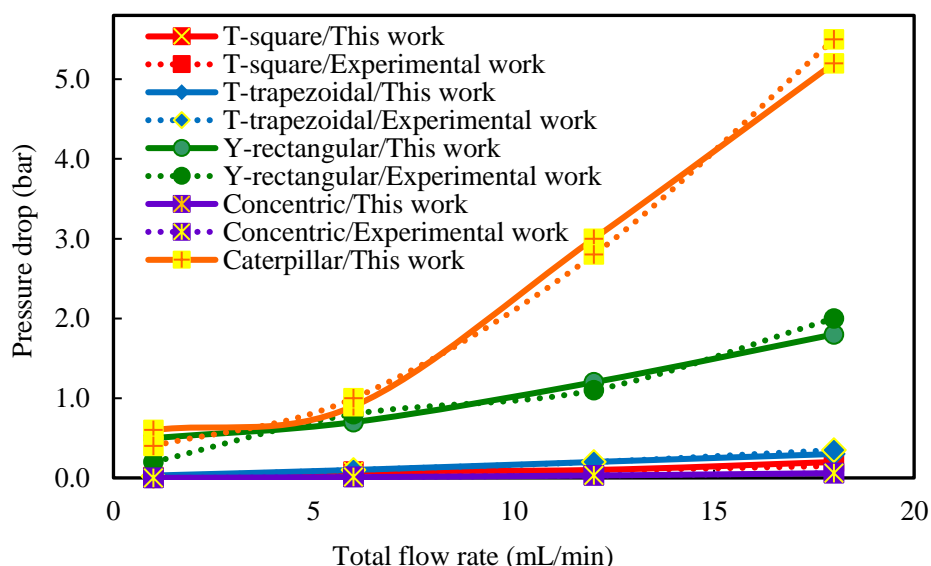
Fig. 2. Effect of liquid flow rates on the average pressure drop for various configurations of MCRs [18]

From Fig. 2, it is apparent that numerical results are almost consistent with the pressure measurements conducted by experiments, indicating the reliability of the simulations. As seen for all configurations of MCRs, both simulation and experimental results exhibit that the pressure drop values are increasing with a rise in the flow rate. However, depending upon the MCR configuration, two kinds of performance are discovered; linear and polynomial. The former is ascribed to the MCRs, which are not equipped with internal structures, whereas the

trend is slightly different for the caterpillar MCR, revealing a nonlinear relationship between the pressure drop measurements and the total liquid flow rate. This is mainly due to the meaningful effect of the mixing zone size, where the two aqueous solutions were contacted on the pressure loss predictions [22]. This means that by raising the values of Reynolds number, as in this study, ranging from 15-2052, depending on MCR configurations, the mixing region enlarges, and the pressure drop substantially rises. Based on the pressure drop plot in Fig. 2, the pressure drop is relatively significant in Y-rectangular MCR, whereas it is negligible in concentric MCR.

To better understand the mixing region, the numerical simulation of the pressure contours was achieved along the mixing channel length for the two different families of the MCRs, including T-square and caterpillar MCRs (Fig. 3). The results of the pressure drop dependencies for the T-square MCR show that at Q_l=1 mL/min, the values of the pressure are slightly decreased with a minimum pressure loss of 0.01 bar, while at higher values of liquid flow rate, O_l= 18 mL/min, a high-pressure loss of ΔP=0.22 bar is observed.
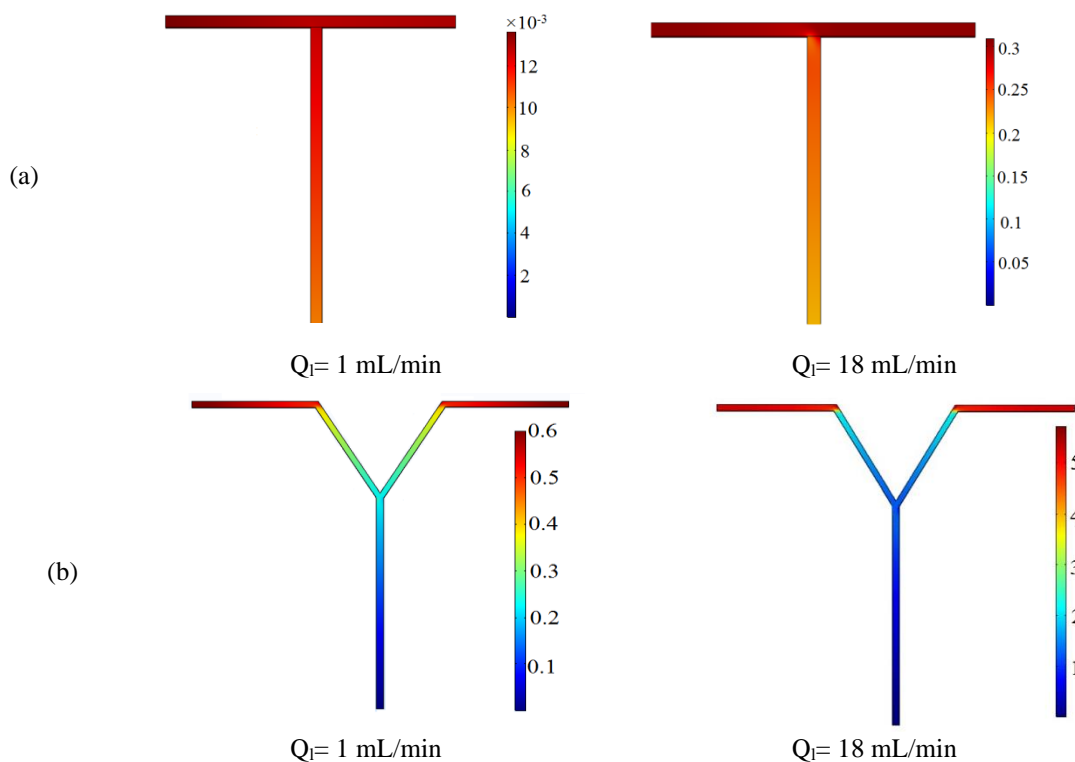
Fig. 3. The pressure contours (bar) for (a) T-square and (b) caterpillar MCRs at a liquid flow rate of Q_l= 1 and 18 mL/min

The observed trend for caterpillar MCR is slightly different from that of the T-square design; compared with the T-square, the caterpillar MCR shows considerably more pressure loss throughout the liquid flow rate range. As for Q_l=1 mL/min, corresponding to the Re No of 15, the pressure drop in the studied micromixer is about ΔP=0.6 bar, increasing the liquid flow rate to 18 mL/min (Re No.~279) significantly influences the pressure loss to ΔP= 5.2 bar. This means that high energy input is required for the flow deflection into the caterpillar MCR. Therefore, a balance between the micromixing quality and energy requirement must be considered when designing such MCRs.

Effect of the Flow Rate on Energy Dissipation

As the fluid streams from two arms of MCR are introduced, mixing occurs with energy consumption, which is sensed by pressure drop. In this regard, an energy dissipation model appears to be the only pertinent parameter to outline an efficient micromixer; the energy dissipation quantifies the micromixing performance as a function of operating conditions [23]. The energy dissipation rate per unit mass of fluid, ε (W/kg), was calculated from the pressure loss and the flow, as stated in the following equation:

$$\varepsilon = \frac{Q\Delta P}{\rho_l V_m} \qquad (16)$$

where Q and ΔP represent the volumetric flow rate (m^3/s), and the pressure drop (N/m^2) obtained from simulation results, respectively, ρ_l implies the liquid density (kg/m^3), and V_m denotes the liquid volume over which the energy is dissipated (m^3) [24]. The values of the specific energy dissipation (ε) through each MCR are plotted logarithmically over the respective inlet flow rates in Fig. 4.
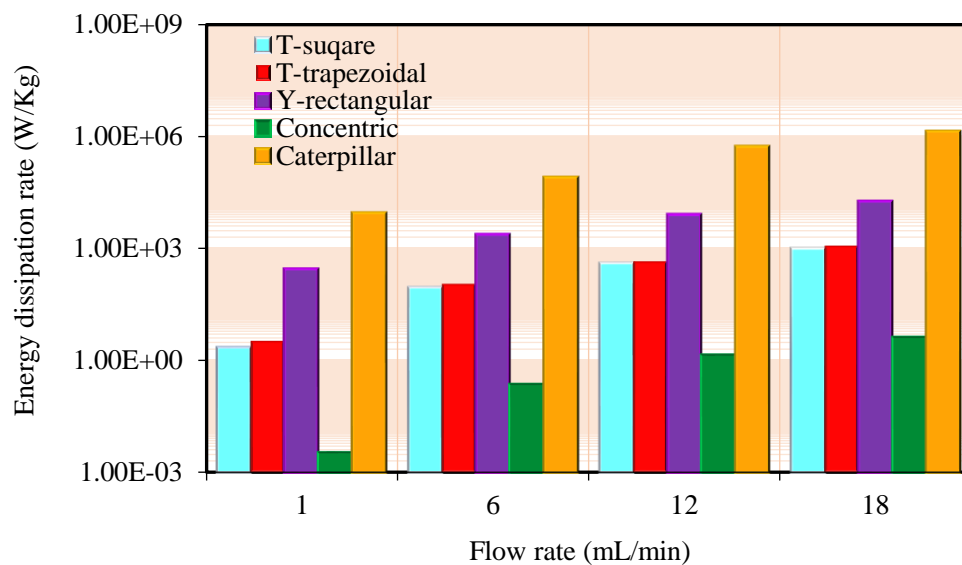
Fig. 4. Effect of flow rate on the specific energy dissipation for five generic MCRs

From the figure, it is recognized that with an increase in the liquid flow rate, the required energy input will grow dramatically in the order of 2.2-1.34 E6 W/kg. This is mainly due to the fact that increasing the flow rate makes vortices in the MCR, thus resulting in the enhancement of mixing performance [16]. Comparing the energy dissipated in the MCRs illustrates that the energy dissipation for caterpillar design is higher than those of other configurations. As an illustration, at the minimum flow rate of 1 mL/min, the caterpillar microchannel consumes energy almost 6 orders of magnitude higher in comparison to the concentric microchannel. The next four generic microchannels display a similar trend with slightly low specific energy dissipation compared to the caterpillar design. In general, the order of the energy dissipation rate is as Caterpillar > Y-rectangular > T-trapezoidal >T-square > Concentric, which is in agreement with the literatures [25]. In addition, the two T-square and T-trapezoidal MCRs display nearly similar energy dissipation rates at various liquid flow rates, as the variation of ε in terms of the liquid flow rate is very coincident with the calculated trend for pressure drop.

Mixing Time (t_m)

Mixing time (t_m), as a valid parameter for evaluating the mixing performance in MCRs, can also be declared as a function of the energy dissipation (ε). Incorporation model was employed for estimating the micromixing time of microchannel reactors using linear growth function for acid volume [18, 26]. In Fig. 5, the mixing time was calculated for five MCRs from the following power-law relation [16]:

$$t_m = a\varepsilon^b \tag{17}$$

where a, and b are constants, as displayed in Fig. 5. The mixing time results, calculated for five MCRs, reveal that increasing the energy dissipation will decline the micromixing time.
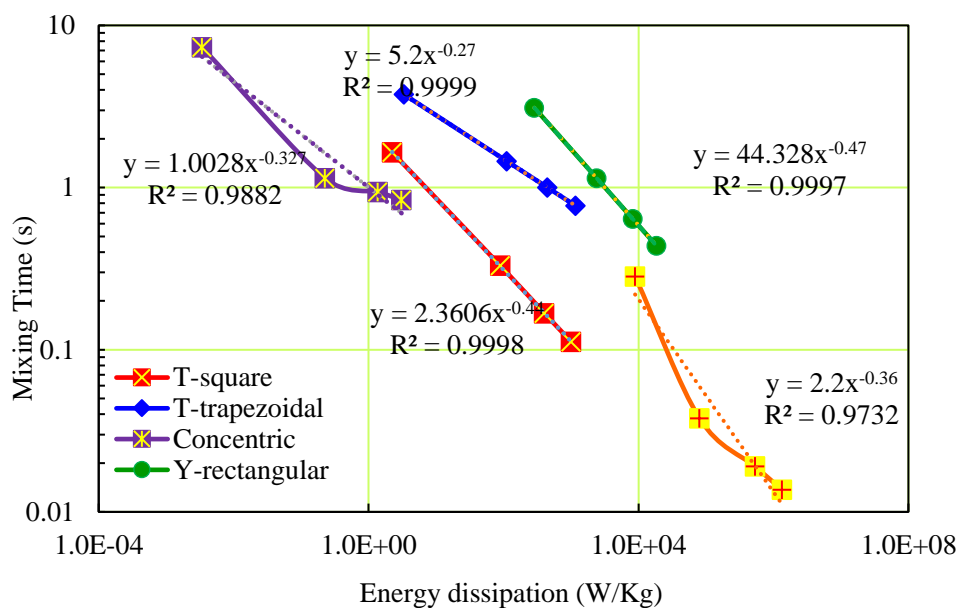
Fig. 5. The theoretical micromixer mixing time results as a function of specific energy dissipation in five generic MCRs

Based on the reported results, the micromixing time scales are in the range of 0.01-10 s, depending on the MCR geometry. The low values of mixing time for caterpillar MCR are found in the range of 0.01-0.1 s for the liquid flow rate of 1-18 mL/min. The better performance of the caterpillar configuration is mainly attributed to the small diameter size, producing recirculation flows crossing to the streamline. The Y- and the T-trapezoidal microchannels present the same order of mixing time in the range of 0.1-10 s, which is one order of magnitude higher than the caterpillar design. The mixing time in the concentric MCR was also two orders of magnitude higher than the caterpillar micromixer, indicating the nearly inferior performance of the mentioned MCR.

To further assess the effect of liquid flow rate on the final micromixing time, the micromixing time versus liquid flow rate was indicated in Fig. 6 for the five configurations of the MCR. The results reveal that the micromixing time relies more on the channel configuration than the liquid flow rate, especially at high liquid flow rates of 18 mL/min. As illustrated, in the case of the caterpillar design, by increasing the liquid flow rate from 1 to 18 mL/min, the mixing time improves by approximately 20.7 times, while at a high liquid flow rate of 18 mL/min, comparing the mixing time of the two MCRs, including concentric and caterpillar,

shows that the mixing time improves by approximately 61 times. As such, the effect of the MCR layouts on the mixing time is more noticeable than the liquid flow rate.
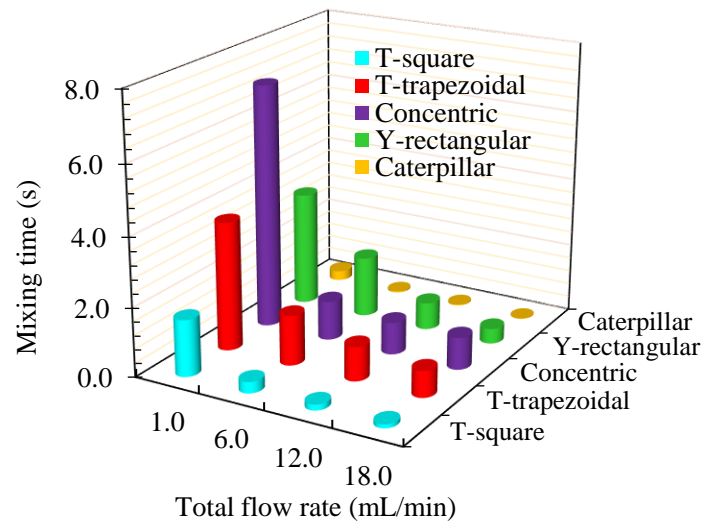
Fig. 6. The mixing time (t_m) versus total flow rate for different MCRs

Furthermore, the increased liquid flow rate augments the micromixing time, as expected. The reason is that the higher turbulence intensities will be achieved at high liquid flow rates inside the MCR [23]. On the other side, increasing the liquid flow rate will intensify the injection velocity, resulting in a more violent collision and a higher specific energy dissipation rate inside the impingement region of the MCR.

Segregation Index (X_s)

The impact of the MCR geometry on the enhancement of the micromixing performance was explored in terms of the segregation index in Fig. 7. As indicated in Fig. 7, the segregation index is generally in the range of 0.002-0.025. Although the outcomes of the model prediction illustrate non-significant differences in the predicted segregation index inside the five generic designs, when compared with the published laboratory data [18], the magnitude order of X_s allows a qualitative judgment on the five studied MCRs. While the predicted range of X_s values for caterpillar, concentric, and Y-rectangular designs are lower than the experimental segregation index, the model overestimates the X_s values for T-microchannels, originating from the error in prediction of the respective mixing time (See also Fig. 8).

(a)   (b)
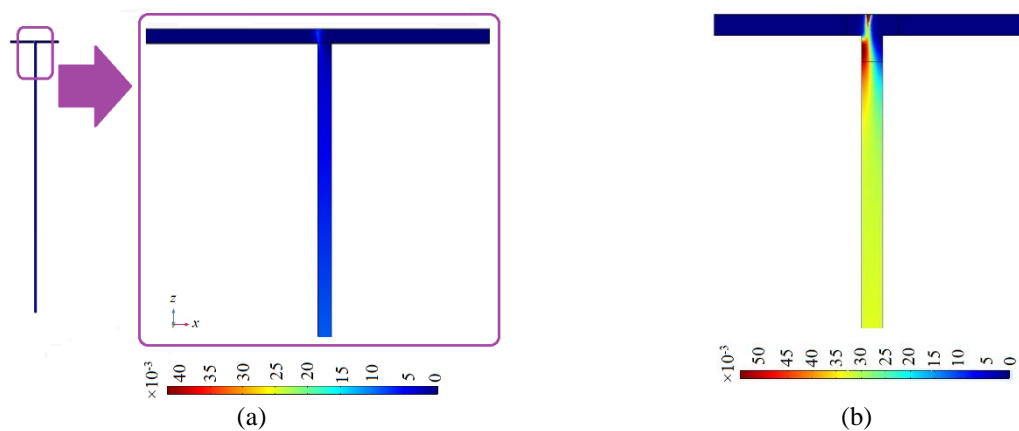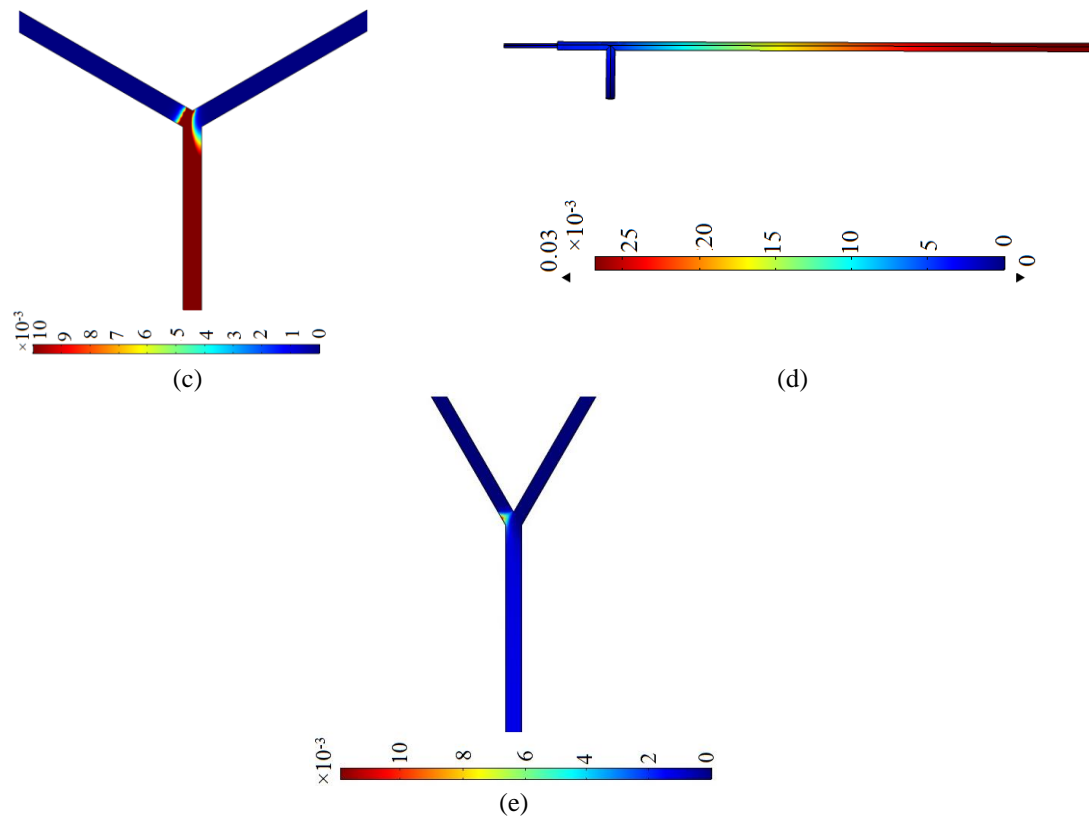
Fig. 7. Comparison of contour plots of segregation index (X_s) for different MCRs at a liquid flow rate of $Q_l=1$ mL/min: (a) T-square (b) T-trapezoidal (c) Y-rectangular (d) Concentric (e) Caterpillar

As shown in Fig. 7a, under the studied volume flow rate, the micromixing is almost finalized at the impingement junction area, as the X_s additionally declines only marginally along the channel outlet close to the impingement area. Accordingly, the rest of the outlet channel has an insignificant influence on the segregation index. Nevertheless, for concentric design, the MCR outlet length has a significant impact on achieving complete micromixing. Considering this, the length of the MCR requires to be fixed at the optimal value to avoid the unneeded length of the MCR in the factual efficient micromixing process.

A comparison of segregation index values at a constant typical liquid flow rate illustrates that the caterpillar configuration gives the best mixing performance (X_s ~0.0024), followed by T-square and Y-rectangular designs with X_s~ 0.0061 and 0.0161, respectively. The low diameter of the caterpillar design suggests playing a significant role in explaining the order of micromixing performance for the MCRs with this range of dimensions. In the case of T-microchannels, the hydraulic diameter of the T-square and T-trapezoidal designs are the same, and the simultaneous impact of inlet streams coming from opposite directions, making the fluid-fluid collision impact maximum, is common to both. Nevertheless, the T-square design gives a better micromixing performance. The reason comes from the non-symmetry of the cross-section of the former MCR, resulting in nearly poor mixing. A similar trend was seen for other volume flow rates when the other operating conditions were maintained constant.

The effect of flow rate on the segregation index was investigated by CFD modeling from 1 to 18 mL/min. Fig. 8 compares the obtained values of X_s at the MCRs outlet for four different liquid flow rates. As can be noticed, CFD results have a good visual agreement with the earlier experimental observations.
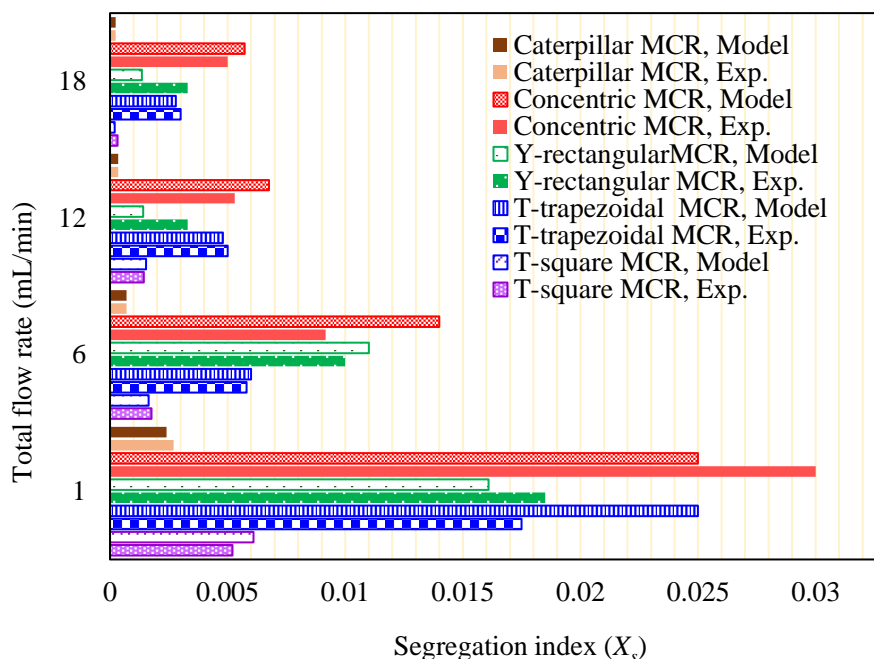
Fig. 8. Comparison of segregation index (X_s) with different flow rates

The general trend of the results demonstrates that increasing the liquid flow rate generally augments the micromixing performance, as expected. This trend can be discussed from two aspects; The first reason is mainly due to the fact that at low Reynolds numbers, where the flow is laminar, as it was in this study ($Re = \dfrac{d_{inlet} U_{inlet}}{v} \sim 15\text{-}2052$), the mixing is thoroughly due to molecular diffusion between the layers of various concentrations. When the volume flow rate rises, the size of liquid elements is expected to be smaller, and convoluted convection-dominated mixing mechanisms are inspected so that a strong flow impinging is produced in the convergence region [27]. The generated velocity heightens the contact area of the reactants and shortens the mixing distance. The other reason is that increasing the liquid flow rate for the same conditions will increase the energy dissipation and decline the micromixing time scale, as well. As such, the high flow rates are favorable for the micromixing in the designed MCRs.

The Mass Fraction of the Byproducts

The first mixing zone, where the two streams contact each other, has a significant impact on the final micromixing efficiency. Moreover, the competition of the mixing and reaction in the first contact region determines the actual reaction rate. Therefore, the mass fraction of the generated and accumulated by-product in the first contact region determines the micromixing efficiency.

Fig. 9 depicts the mass fraction of the by-product ($I_2+I_3^-$), computed at four various total flow rates in the caterpillar MCR.
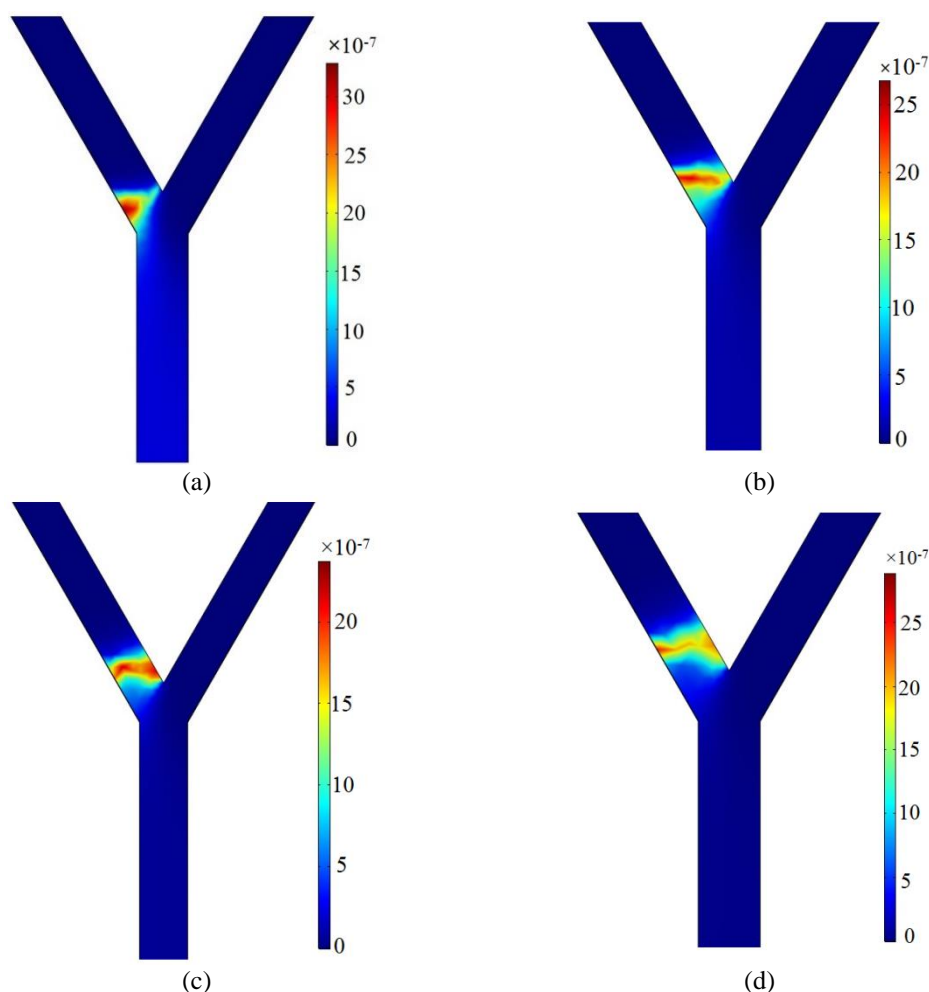
Fig. 9. Comparison of the mass fraction of the sum of I_2 and I_3^- (by-products) for caterpillar design with different total flow rates a) $Q_l=1$ mL/min, b) $Q_l=6$ mL/min, c) $Q_l=12$ mL/min, d) $Q_l=18$ mL/min

As specified in this figure, for the same acid concentration, I_2 and I_3^- are produced at the left entrance of the caterpillar MCR, near the impingement point with a maximum mass fraction of 30×10^{-7}. Besides, the CFD contour results suggest that the maximum values of the $(I_2+I_3^-)$ slightly decreased to 20×10^{-7} as the total liquid flow rate was set to 18 mL/min. This phenomenon is mainly due to the effective mixing achieved at higher velocities and was previously examined for mixing in MCRs [28].

Accordingly, at a low total liquid flow rate, the by-products would be easily generated and accumulated, which is attributed to the slower mixing process. This result confirms that the high values of the X_s are obtained at low liquid flow rates. On the other hand, a longer channel length requires achieving the same micromixing performance in the same caterpillar MCR. In the case of Fig. 9d at the liquid flow rate of 18 mL/min, the results show that for the same inlet acid concentration, the mass fraction of the by-product accumulated in the MCR is relatively small, resulting in lower X_s and better micromixing condition in the studied MCR.

Conclusion

The micromixing process of five generic microchannels with various geometric constructions was described by CFD simulation. The competitive iodide-iodate reaction system was applied to demonstrate the micromixing characterization, concerning the mixing time,

energy dissipation, segregation index, and the mass fraction of the various species under different flow rates of 1-18 mL/min. Evaluation of micromixing time in terms of the energy dissipated in the MCRs ranked the caterpillar design with 150 μm internal diameter as the most efficient micromixer. The concentric configuration with a diameter of 1600 μm was also discerned the least efficient configuration among the studied micromixers.

The outcomes of the segregation index revealed that the segregation index is substantially sensitive to the volumetric flow rate, and increasing the flow rate when the other conditions are the same, is favorable for X_s of the designed MCRs. The CFD contour results of the mass fraction of the by-product ($I_2+I_3^-$) also suggested that the by-products would be easily generated and accumulated at low total liquid flow rates. Finally, the superior performance of the caterpillar design was demonstrated in terms of the micromixing time, estimated as 0.013-0.083 s within the Re No. of 15-279, corresponding to the X_s of 0.0002-0.002. While the Y- and the T-trapezoidal MCRs present the same order of mixing time in the range of 0.1-10 s, the mixing time in the concentric MCR was two orders of magnitude higher than the caterpillar micromixer.

References

[1]   Arian E, Pauer W. Sucrose solution as a new viscous test fluid with tunable viscosities up to 2 Pas for micromixing characterization by the Villermaux–Dushman reaction. Journal of Flow Chemistry. 2021;11(3):579-88.

[2]   Manzano Martínez AN, Haase AS, Assirelli M, van der Schaaf J. Alternative Kinetic Model of the Iodide–Iodate Reaction for Its Use in Micromixing Investigations. Industrial & Engineering Chemistry Research. 2020;59(49):21359-70.

[3]   Ouyang Y, Xiang Y, Gao X-Y, Zou H-K, Chu G-W, Agarwal RK, et al. Micromixing efficiency optimization of the premixer of a rotating packed bed by CFD. Chemical Engineering and Processing-Process Intensification. 2019;142:107543.

[4]   Cheng K, Liu C, Guo T, Wen L. CFD and experimental investigations on the micromixing performance of single countercurrent-flow microchannel reactor. Chinese Journal of Chemical Engineering. 2019;27(5):1079-88.

[5]   Fonte CP, Fletcher DF, Guichardon P, Aubin J. Simulation of micromixing in a T-mixer under laminar flow conditions. Chemical Engineering Science. 2020;222:115706.

[6]   Clark J, Kaufman M, Fodor P. Mixing Enhancement in Serpentine Micromixers with a Non-Rectangular Cross-Section. Micromachines. 2018;9(3):107.

[7]   Hossain S, Afzal A, Kim K-Y. Shape optimization of a three-dimensional serpentine split-and-recombine micromixer. Chemical Engineering Communications. 2017;204(5):548-56.

[8]   Fletcher D, Avila M, Poux M, Xuereb C, Aubin J. CFD Modelling of Micromixing in a T-mixer with Square Bends. Conference CFD Modelling of Micromixing in a T-mixer with Square Bends.

[9]   Frey T, Schlütemann R, Schwarz S, Biessey P, Hoffmann M, Grünewald M, et al. CFD analysis of asymmetric mixing at different inlet configurations of a split-and-recombine micro mixer. Journal of Flow Chemistry. 2021;11(3):599-609.

[10]   Wang D, Ye G, Mai J, Chen X, Yang Y, Li Y, et al. Novel micromixer with complex 3D-shape inner units: Design, simulation and additive manufacturing. Computer Modeling in Engineering & Sciences, 123 (3). 2020:1061-77.

[11]   Zhendong L, Yangcheng L, Jiawei W, Guangsheng L. Mixing characterization and scaling-up analysis of asymmetrical T-shaped micromixer: Experiment and CFD simulation. Chemical Engineering Journal. 2012;181:597-606.

[12]   Bertrand M, Lamarque N, Lebaigue O, Plasari E, Ducros F. Micromixing characterisation in rapid mixing devices by chemical methods and LES modelling. Chemical Engineering Journal. 2016;283:462-75.

[13]   Ouyang Y, Xiang Y, Zou H, Chu G, Chen J. Flow characteristics and micromixing modeling in a microporous tube-in-tube microchannel reactor by CFD. Chemical Engineering Journal. 2017;321:533-45.

[14]   Li W, Xia F, Qin H, Zhang M, Li W, Zhang J. Numerical and experimental investigations of

micromixing performance and efficiency in a pore-array intensified tube-in-tube microchannel reactor. Chemical Engineering Journal. 2019;370:1350-65.

[15] Guo M, Hu X, Yang F, Jiao S, Wang Y, Zhao H, et al. Mixing Performance and Application of a Three-Dimensional Serpentine Microchannel Reactor with a Periodic Vortex-Inducing Structure. Industrial & Engineering Chemistry Research. 2019;58(29):13357-65.

[16] Rahimi M, Aghel B, Hatamifar B, Akbari M, Alsairafi A. CFD modeling of mixing intensification assisted with ultrasound wave in a T-type microreactor. Chemical Engineering and Processing: Process Intensification. 2014;86:36-46.

[17] Ouyang Y, Xiang Y, Gao X-Y, Zou H-K, Chu G-W, Agarwal RK, et al. Micromixing efficiency optimization of the premixer of a rotating packed bed by CFD. Chemical Engineering and Processing - Process Intensification. 2019;142:107543.

[18] Kashid M, Renken A, Kiwi-Minsker L. Mixing efficiency and energy consumption for five generic microchannel designs. Chemical engineering journal. 2011;167(2-3):436-43.

[19] Guichardon P, Falk L, Villermaux J. Extension of a chemical method for the study of micromixing process in viscous media. Chemical Engineering Science. 1997;52(24):4649-58.

[20] Rahimi M, Azimi N, Parsamogadam MA, Rahimi A, Masahy MM. Mixing performance of T, Y, and oriented Y-micromixers with spatially arranged outlet channel: evaluation with Villermaux/Dushman test reaction. Microsystem Technologies. 2017;23(8):3117-30.

[21] Unadkat H, Nagy Z, Rielly C. Investigation of turbulence modulation in solid–liquid suspensions using parallel competing reactions as probes for micro-mixing efficiency. Chemical Engineering Research and Design. 2013;91(11):2179-89.

[22] Soleymani A, Kolehmainen E, Turunen I. Numerical and experimental investigations of liquid mixing in T-type micromixers. Chemical Engineering Journal. 2008;135:S219-S28.

[23] Nie A, Gao Z, Xue L, Cai Z, Evans GM, Eaglesham A. Micromixing performance and the modeling of a confined impinging jet reactor/high speed disperser. Chemical Engineering Science. 2018;184:14-24.

[24] Falk L, Commenge J-M. Performance comparison of micromixers. Chemical Engineering Science. 2010;65(1):405-11.

[25] Jafari O, Rahimi M, Kakavandi FH. Liquid–liquid extraction in twisted micromixers. Chemical Engineering and Processing: Process Intensification. 2016;101:33-40.

[26] Fournier M-C, Falk L, Villermaux J. A new parallel competing reaction system for assessing micromixing efficiency—determination of micromixing time by a simple mixing model. Chemical Engineering Science. 1996;51(23):5187-92.

[27] Benz K, Jäckel KP, Regenauer KJ, Schiewe J, Drese K, Ehrfeld W, et al. Utilization of micromixers for extraction processes. Chemical Engineering & Technology: Industrial Chemistry-Plant Equipment-Process Engineering-Biotechnology. 2001;24(1):11-7.

[28] Rahimi M, Valeh-e-Sheyda P, Zarghami R, Rashidi H. On the mixing characteristics of a poorly water soluble drug through microfluidic-assisted nanoprecipitation: Experimental and numerical study. The Canadian Journal of Chemical Engineering. 2018;96(5):1098-108.